

# Heterogeneous Exciton Dynamics Revealed by Two-Dimensional Optical Spectroscopy<sup>†</sup>

Igor Stiopkin,<sup>‡</sup> Tobias Brixner,<sup>‡</sup> Mino Yang,<sup>§</sup> and Graham R. Fleming\*

Department of Chemistry and QB3 Institute University of California, Berkeley, Physical Biosciences Division, Lawrence Berkeley National Laboratory, Berkeley, California 94720-1460, Physikalisches Institut, Universität Würzburg, Am Hubland 97074, Würzburg, Germany, and Department of Chemistry and Institute for Basic Sciences Research, Chungbuk, National University, Cheongju 361-763, South Korea

Received: May 10, 2006; In Final Form: July 26, 2006

We show that optical two-dimensional (2D) spectroscopy can recover ultrafast heterogeneous dynamics of closely spaced delocalized exciton states from a molecular exciton manifold characterized by a single absorption band. The complete experimental third-order nonlinear optical response from room-temperature J-aggregates in liquid phase is reproduced for the first time with self-consistent Frenkel exciton theory combined with modified Redfield theory. We show that exciton relaxation between the exciton states and nuclear-motion-induced exchange-narrowed energy fluctuations of individual delocalized exciton states can be distinguished because these two processes lead to a distinctively different evolution of the absolute 2D spectrum. Our technique also allows recovery of the variation of the exciton relaxation rates as well as the degree of exciton delocalization across the absorption band.

## Introduction

Heterogeneous dynamics is ubiquitous in multilevel systems. Nanostructures such as nanotubes,<sup>1</sup> nanorods,<sup>2</sup> and quantum dots<sup>3</sup> as well as molecular aggregates<sup>4,5</sup> and some peptides<sup>6</sup> are characterized by manifolds of exciton states. In such systems, phonon-induced fluctuation dynamics of exciton states as well as relaxation (hopping) between the states varies across the absorption band. Ultrafast relaxation dynamics of such systems can be studied with pump–probe spectroscopy when the absorption spectrum has distinct bands. Heterogeneous relaxation dynamics on a slower picosecond scale can be recovered with frequency-domain techniques in systems with featureless absorption spectra.<sup>7</sup> However, ultrafast heterogeneous dynamics in such systems is conventionally averaged over the distribution with ultrafast time-domain techniques,<sup>8</sup> and the cumulative effect of both fluctuation and relaxation dynamics are observed. We demonstrate that 2D spectroscopy<sup>9–14</sup> has the capability of recovering variations in both ultrafast relaxation (hopping) between the exciton states and the fluctuation dynamics of the states within the single absorption band of the exciton manifold. Two-dimensional spectroscopy has been recently used to study heterogeneous dynamics of water<sup>15,16</sup> as well as molecular aggregates<sup>4</sup> and peptides<sup>6</sup> containing distinctive features (bands) in the absorption spectra. In this work, we study the ultrafast heterogeneous dynamics of room-temperature J-aggregates, which are linear strongly coupled molecular aggregates representing a chemical analogue of photosynthetic light-harvesting complexes, in particular, the chlorosome.<sup>17</sup> The featureless narrow absorption band of J-aggregates is comprised of a manifold of congested delocalized exciton states. Scattering on static energetic disorder localizes the states on segments smaller than the physical length of the aggregate, and the extent of delocalization of the exciton states varies significantly across

the band. Interaction with phonons produces relaxation between the exciton states as well as fluctuation of the exciton energy levels.

In this paper, we study ultrafast heterogeneous dynamics of room-temperature 1,1'-diethyl-3,3'-bis(sulfopropyl)-5,5',6,6'-tetrachlorobenzimidacarbocyanine (BIC) J-aggregates in aqueous solution with 2D spectroscopy. We reproduce, for the first time, the complete experimental third-order optical nonlinear response of J-aggregates with self-consistent exciton theory.<sup>18</sup> In this theory, states from the one- and two-exciton bands are recovered from an electrostatic Frenkel Hamiltonian. The nuclear-motion-induced electron–phonon coupling Hamiltonian is partitioned into a diagonal part (describing exciton energy fluctuations) and an off-diagonal part. The latter is treated perturbatively with modified Redfield theory<sup>18,19</sup> as a relaxation matrix, leading to a redistribution of the population of exciton states. Additional dephasing induced by population transfer, called “lifetime broadening”, is also included in calculations of the third-order nonlinear response from J-aggregates. We show that exciton relaxation between the exciton states on one hand and nuclear-motion-induced exchange-narrowed energy fluctuations of individual delocalized exciton states on the other lead to different evolutions of the 2D spectrum. Our technique also allows recovery of the variation of the exciton relaxation rates as well as exciton delocalization across the absorption band.

## Experimental Section

Our experimental implementation of 2D spectroscopy for electronic transitions is described in detail elsewhere.<sup>20,21</sup> Briefly, 40 fs, 596 nm pulses at 3 kHz repetition were split into two replicas, one of which can be delayed by a conventional translation stage. The two beams were focused on a diffractive optics element, and the  $\pm 1$  orders of diffraction from each beam were focused into the sample by a concave spherical mirror. Three beams (1–3) were used as pump pulses, while beam 4, attenuated by  $\sim 10^{-4}$ , was used as the local oscillator. The photon echo signal was detected in the  $\mathbf{k}_s = -\mathbf{k}_1 + \mathbf{k}_2 + \mathbf{k}_3$  phase-matched direction, and a box geometry was used. Reference beam 4, collinear with the signal, arrived  $\sim 609$  fs

<sup>†</sup> Part of the special issue “Charles B. Harris Festschrift”.

\* Corresponding author. E-mail: GRFleming@lbl.gov.

<sup>‡</sup> Physikalisches Institut, Universität Würzburg.

<sup>§</sup> Department of Chemistry and Institute for Basic Sciences Research, Chungbuk, National University.

before the signal to eliminate pump–probe contributions.<sup>21</sup> Spectral interference fringes between the signal and the reference beams were recorded with a spectrometer equipped with a CCD detector. The spectral interferometry technique recovered the complete electric field magnitude and phase of the signal from a single CCD reading. The scattered pump light from the sample cell propagating in the reference beam direction was subtracted with an automated shutter.<sup>20,21</sup> A symmetric scanning method was used to remove the discontinuity in the signal around time  $\tau = 0$ .<sup>9,20,21</sup>

Pump pulse intensities below  $10^{12}$  photons/(pulse  $\text{cm}^2$ ) were used to minimize the effect of exciton–exciton annihilation.<sup>22</sup> Beams were focused into a  $100\ \mu\text{m}$  spot on a  $100\ \mu\text{m}$  thick flow sample cell. Absorption was adjusted to 0.15 OD at peak value. The J-aggregate solution was prepared by dissolving 1,1'-diethyl-3,3'-bis(sulfoethyl)-5,5',6,6'-tetrachlorobenzimidacarbocyanine (BIC) dye in filtered deionized water at ambient temperature.

We model the J-aggregate as a linear assembly of  $N$  two-electronic-level molecules with parallel transition dipole moments via the Frenkel Hamiltonian.<sup>8,18,23</sup> Phonon-induced energy fluctuations of the molecular electronic states were induced via generalized nuclear coordinate  $q$ :

$$H(q) = \sum_{n=1}^N \epsilon_n B_n^+ B_n + \sum_{\substack{m,n=1 \\ m \neq n}}^N J_{mn} B_m^+ B_n + \sum_{n=1}^N H_{nn}^{\text{el-ph}}(q) B_n^+ B_n + H^{\text{ph}}(q) \quad (1)$$

$B_n^+$  ( $B_n$ ) are exciton creation (annihilation) operators connecting the ground  $|0\rangle$  and the excited  $|n\rangle$  electronic states of the  $n$ th molecule.<sup>18</sup> The monomer electronic transition energies,  $\epsilon_n$ , are normally distributed by the static disorder.  $J_{mn}$  is the magnitude of electrostatic transition dipole–dipole coupling between monomers  $m$  and  $n$  and is assumed to be nuclear coordinate ( $q$ ) independent. Interaction of the electronic states with phonons is mediated by the electron–phonon coupling Hamiltonian  $H^{\text{el-ph}}(q)$ , which is assumed to be diagonal,<sup>8,18</sup> as solvent-mediated correlations of energy fluctuations between neighboring monomers are relatively weak.  $H^{\text{ph}}(q)$  is the phonon Hamiltonian.

Exciton states  $|k\rangle = \sum_{n=1}^N \varphi_{kn} |n\rangle$  comprising the one-exciton manifold are defined as eigenstates of the electrostatic part of Hamiltonian in eq 1 (first two terms). These states are delocalized over segments of the aggregate chain, and the extent of delocalization of the exciton  $|k\rangle$  is approximately  $L_{\text{DEL}}(k) = 1/\sum_{n=1}^N |\varphi_{kn}|^4$  monomers (note  $1 \leq L_{\text{DEL}}(k) \leq N$ ). The one-exciton Hamiltonian in the  $|k\rangle$  basis becomes:

$$H(q) = \sum_{k=1}^N |k\rangle E_k \langle k| + \sum_{k,k'=1}^N |k\rangle H_{kk'}^{\text{ex-ph}}(q) \langle k'| + H^{\text{ph}}(q) \quad (2)$$

In the exciton basis,  $|k\rangle$ , the electron–phonon Hamiltonian  $H^{\text{el-ph}}(q)$  is not diagonal. We will call the electron–phonon Hamiltonian  $H^{\text{el-ph}}(q)$  in the exciton basis the exciton–phonon coupling Hamiltonian,  $H_{kk'}^{\text{ex-ph}}(q)$ . Its off-diagonal component,  $H_{kk'}^{\text{ex-ph}}(q)$ , induces relaxation between the exciton states  $|k\rangle$  and  $|k'\rangle$ . The diagonal component,  $H_{kk}^{\text{ex-ph}}(q)$ , defines the nuclear-motion-induced fluctuation of the energy gap between the ground state and the exciton state  $|k\rangle$ . The electron–phonon coupling Hamiltonian  $H_{kk}^{\text{ex-ph}}(q)$  is linear in the nuclear coordinate

$q$ , as we assumed  $H_{nn}^{\text{el-ph}}(q_n) \sim q_n$ . The off-diagonal exciton–phonon coupling is described with a modified form of Redfield theory.<sup>18,19</sup> A master equation with relaxation rates predicted by the modified Redfield theory is numerically solved to simulate population dynamics of exciton states within the one-exciton manifold.<sup>8</sup> Additional dephasing produced by the exciton relaxation, the so-called “lifetime broadening”,<sup>8</sup> is included in our calculation. All Feynman diagrams surviving the rotating wave approximation<sup>9</sup> for our phase-matching condition are included in calculations of the third-order nonlinear response  $R^{(3)}$ .<sup>8</sup> These diagrams include the ground state and the states from one-exciton and two-exciton bands. The states from the second exciton band were obtained by numerical diagonalization of the second exciton band Hamiltonian and not by analytical formulas from the Bethe Ansatz<sup>18</sup> because we have also included nonnearest neighbor electrostatic dipole–dipole coupling into the Hamiltonian in eq 1. Coherence transfer induced by the off-diagonal exciton–phonon coupling Hamiltonian  $H_{kk'}^{\text{ex-ph}}(q)$  was not included. We expect coherence transfer to influence the third-order nonlinear response at short ( $T \leq 50$  fs) population periods.

The 2D spectra were calculated from the full third-order polarization  $P^{(3)}(\tau, T, t)$  via double Fourier transformation.

$$S^{(3)}(\omega_\tau, T, \omega_t) = \int \int d\tau dt e^{i\omega_\tau \tau} e^{i\omega_t t} P^{(3)}(\tau, T, t) \quad (3)$$

The 2D spectrum  $S^{(3)}(\omega_\tau, T, \omega_t)$  is a complex quantity that can be represented either by the real and the imaginary parts or by absolute value and phase plots depending on the application. The frequency  $\omega_\tau(\omega_t)$  corresponds to the first (last) coherence time interval  $\tau$  ( $t$ ) when the photon is absorbed (emitted). Contributions to the polarization  $P^{(3)}(\tau, T, t)$ , including transitions between different states, are centered at different points of the 2D plane  $(\omega_\tau, \omega_t)$ . The width of each contribution in the  $\omega_\tau(\omega_t)$  direction is related to the dephasing rate of this transition. As the population time  $T$  is increased, exciton relaxation between the states as well as nuclear-motion-induced energy gap fluctuations (“spectral diffusion”) change the emission frequency  $\omega_t$ , leading to shifting and broadening of the contribution to the 2D spectrum. These dynamics are reflected in the total J-aggregate spectrum, which contains all nonzero contributions between the ground state and states from the one- and two-exciton bands.

## Results and Discussion

Figure 1 shows experimental and calculated real and imaginary 2D spectra plotted for population times  $T \sim 0, 50, 200$ , and  $\sim 1000$  fs. The experimental spectra were averaged over 7, 8, 6, and 10 scans, respectively. The real part of the 2D spectrum at  $T = 0$  fs (Figure 1) has both positive (solid lines) and negative (dashed lines) peaks. The negative peak can be viewed as excited state absorption and corresponds to the second exciton band contribution to the nonlinear signal. The slope of the nodal line reflects the degree of memory of the initial excitation frequency retained by the system. The imaginary 2D spectrum consists mostly of one positive feature, originating from the cancellation of the oppositely signed dispersion-like (in the  $\omega_t$  direction) one- and two-exciton band contributions to the nonlinear signal. As the population time  $T$  increases, the slope of the nodal line of the real 2D spectrum decays to become almost horizontal. In addition, the relative amplitude of the negative peak is reduced with respect to that of the positive peak. These features reflect the memory loss of the system due to both the exciton population transfer between the exciton states and due to nuclear-motion-

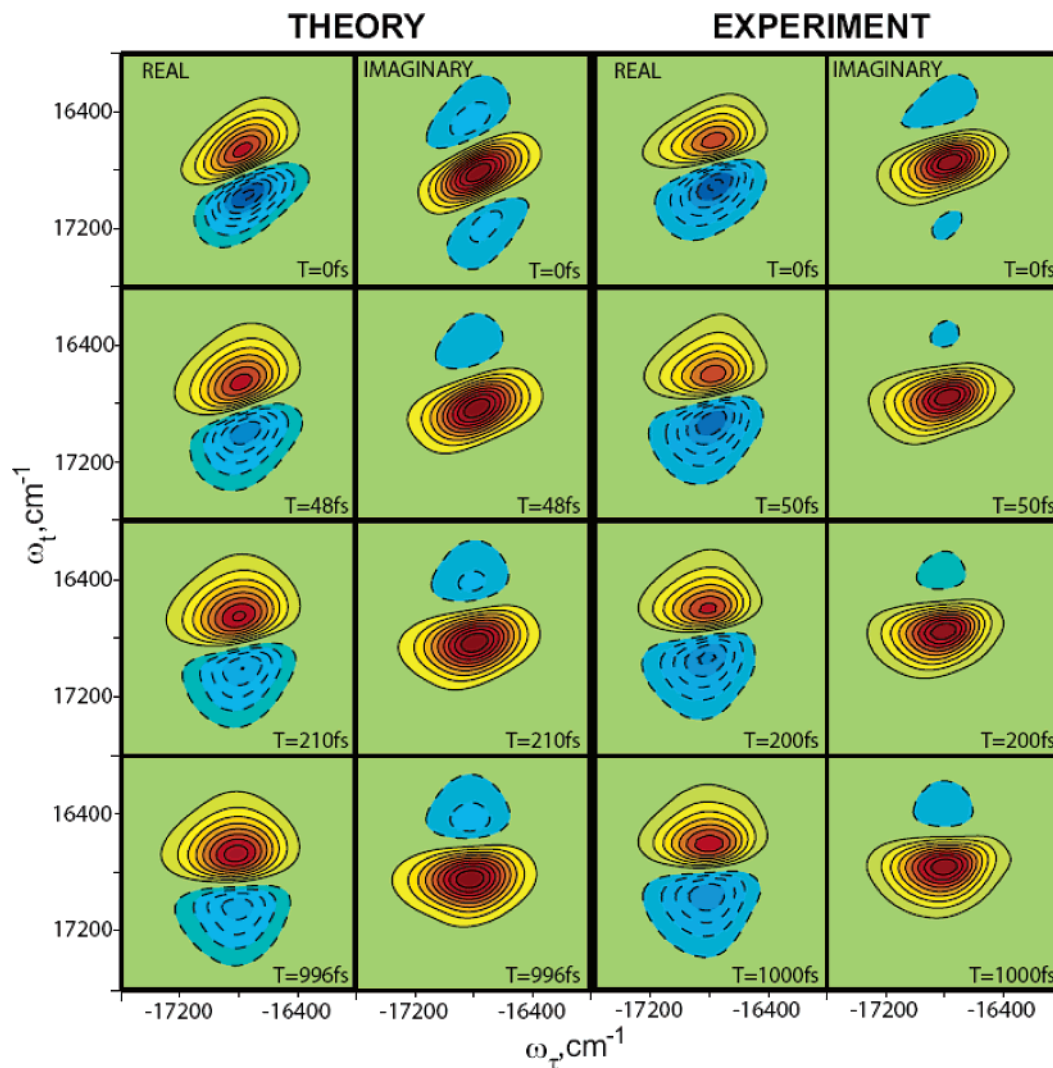


**Figure 1.** Comparison of the theoretical and the experimental third-order nonlinear optical responses from BIC J-aggregates in water. Real and imaginary 2D spectra obtained (left pair) theoretically (see text for parameters) for population times  $T = 0, 48, 210, 996$  fs and experimentally (right pair) for population times  $T = 0, 50, 200, 1000$  fs. Contour lines for each spectrum are plotted at 10, 20, ..., 90% (solid) and -10, ... -90% (dashed) of the peak value of the imaginary 2D spectrum corresponding to that population period. The ratios of the maximum values of the imaginary 2D spectra simulated for  $T = 0, 48, 210$  and  $996$  fs is 1:0.85:0.62:0.53, respectively, while the same ratio for the experimental results is 1:0.74:0.54:0.42 for  $T = 0, 50, 200$  and  $1000$  fs.

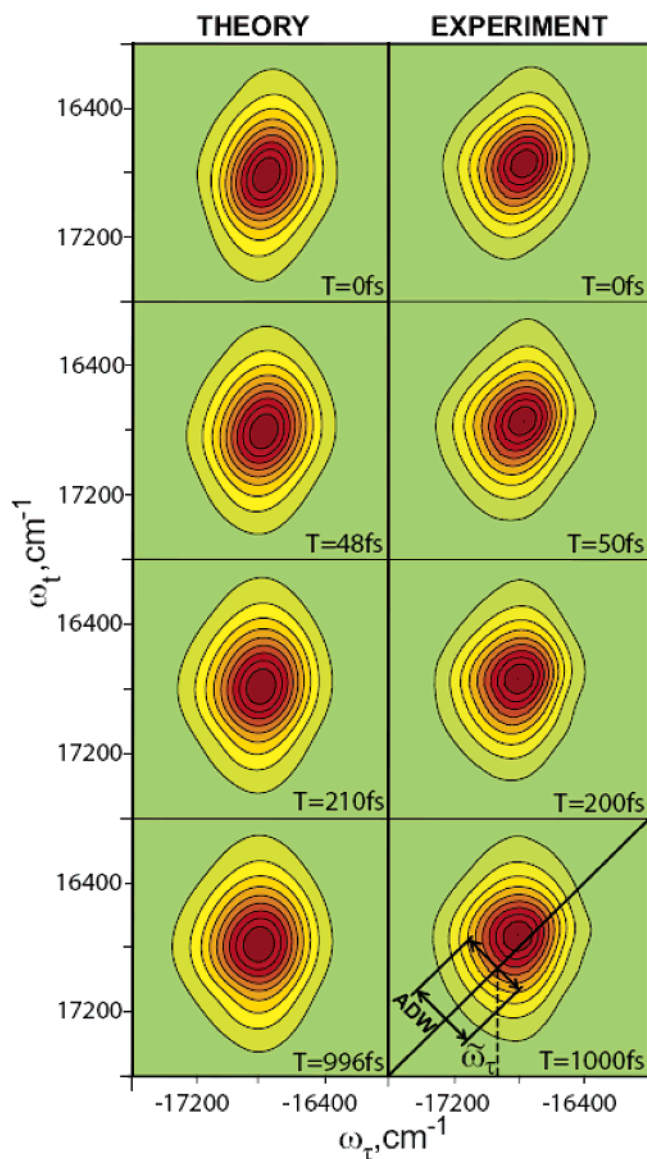
induced energy fluctuations of the individual exciton states. The imaginary 2D spectrum broadens nonuniformly, manifesting strong frequency-dependent exciton dynamics. Rapid broadening of both real and imaginary 2D spectra as well as rapid change in the slope of the nodal line of the real 2D spectrum at short times are mostly induced by processes during the laser pulse overlap period<sup>20,21</sup> and by the fastest components of the exciton relaxation and by the spectral diffusion. At longer times, exciton relaxation can reduce the slope of the nodal line to (or very near to) zero, while spectral diffusion reduces the slope to a finite non-zero value that reflects preservation of memory (inhomogeneous broadening). A detailed discussion of these points will be given in a future publication.

Figure 1 also shows the result of our theoretical modeling of the real and the imaginary 2D spectra. The nonlinear polarization is obtained by convoluting the time-domain response function with the laser pump pulses (31 fs fwhm intensity). The magnitude of the electrostatic dipole-dipole coupling between the nearest neighbors  $J = 1080$  cm<sup>-1</sup> is obtained from the J-aggregate absorption spectrum red-shift of about 2600 cm<sup>-1</sup>.<sup>23</sup> We include in the simulations the electrostatic dipole-dipole coupling between molecules separated by 5 or fewer intermo-

lecular distances. The monomer transition-frequency correlation function is taken as a Gaussian function with reorganization energy strength  $\lambda = 320$  cm<sup>-1</sup> and a time constant  $\tau_g$ .<sup>24</sup> The static disorder in monomer transition energies is assumed to be Gaussian with standard deviation  $\sigma = 270$  cm<sup>-1</sup>. Of the four model parameters  $J$ ,  $\sigma$ ,  $\tau_g$ , and  $\lambda$ , only the values of  $\sigma$  and  $\lambda$  (at fixed value of  $\tau_g$ ) were adjusted to reproduce the J-aggregate absorption spectrum. This absorption spectrum fit provided a constraint on the simultaneous choice of  $\sigma$  and  $\lambda$  (for fixed  $\tau_g$ ). The values of  $\sigma$  and  $\lambda$  were simultaneously adjusted to reproduce the shapes of the experimental real and imaginary 2D spectra. Similar procedures were carried out for  $\tau_g = 30, 50, 70$ , and  $90$  fs. The value of  $\tau_g = 70$  fs produced the best evolution of the absolute 2D spectrum with the population time  $T$  that is most similar to the experimental data.

Calculations of the response function were performed on a chain of 70 monomers. This chain length corresponds to an average energy separation of 75 cm<sup>-1</sup> between the neighboring levels of the one-exciton band. The electrostatic dipole-dipole nonnearest neighbor coupling was included in simulations, as it strongly affects the balance of positive and negative peaks in the real 2D spectrum. A 6 fs step in all time periods was used





**Figure 2.** Theoretical (left) and experimental (right) absolute 2D spectra for BIC J-aggregates in water. Contour lines are plotted at 10, 20, ..., 90% of the peak value. The ratios of the maximum values of the absolute 2D spectra simulated for  $T = 0, 48, 210$  and  $996$  fs is 1:0.86:0.64:0.56, respectively, while the same ratio for the experimental results is 1:0.74:0.54:0.43 for  $T = 0, 50, 200$ , and  $1000$  fs.

in the simulations. The calculated signals were averaged over 500 realizations of the static disorder, which is sufficient for converged results. Slightly faster relaxation and stronger exchange narrowing appeared as the chain was elongated.

The absolute 2D spectrum of J-aggregates is weakly sensitive to the interplay of the balance of the positive and negative one- and two-exciton contributions to the nonlinear signal. This positively signed 2D spectrum allows more direct easy visualization of exciton energy fluctuations and exciton relaxation processes, which cause nonuniform broadening of the 2D spectrum than the real or imaginary spectra, although of course their information content is identical.

Both experimental and theoretically simulated absolute 2D spectra (Figure 2) show similar evolution with increasing population time. During the first 50 fs, the absolute 2D spectra broaden almost uniformly in the direction perpendicular to the diagonal line  $\omega_r = -\omega_t$ . From population times 50–200 fs, the high-frequency portion (lower left) of the absolute 2D spectra broadens more strongly than the low-frequency portion (top

right). As the population time further increases from 200 to  $\sim 1000$  fs, the low-frequency portion of the spectrum broadens more strongly than the high-frequency portion.

We looked for a simple characteristic of 2D spectra that allowed the influence of exciton relaxation and spectral diffusion to be distinguished. Extensive numerical simulations suggested that the antidiagonal width (ADW) of the absolute 2D spectrum, taken at frequency  $\omega_r$  and defined as the width taken at 70% of the maximum of the absolute 2D spectrum cross section, is drawn perpendicular to and crossing the diagonal line at  $\omega_r = -\omega_t$  (see Figure 2). The key point is that exciton relaxation and spectral diffusion influence the high- and low-frequency sides of the spectrum quite differently. Population relaxation is fastest for higher-energy states, leading to differential broadening at higher frequencies. Conversely, spectral diffusion has a greater effect on lower-energy states because exchange narrowing is weakest for these levels.<sup>8</sup> These qualitative comments were confirmed by extensive numerical simulation. Thus the evolution of frequency-dependent antidiagonal width plotted as a function of population time can distinguish between the influence of exciton relaxation and spectral diffusion on the 2D spectrum in a fairly straightforward manner. Plots of the ADW for the experimental data and for the results of simulations are shown in Figure 3. The experimental ADW (Figure 3a) broadens mostly uniformly from  $T = 0$  fs to  $T = 50$  fs. With increasing population time from  $T = 50$ –500 fs, the ADW broadens significantly more strongly at higher frequencies. The higher-frequency region of ADW does not significantly broaden after  $T = 500$  fs, while the low-frequency side significantly broadens between 500 fs and  $T = 1000$  fs. Simulations with the best fit parameters (Figure 3b) show qualitatively similar evolution of the ADW with population time. There is mostly uniform broadening of the ADW with population time increasing from  $T = 0$ –48 fs; the high-frequency part of the ADW broadens significantly when  $T$  increases to 210 fs, while the low-frequency portion of the ADW curve increases significantly more than the high-frequency region at longer population times.

A precise determination of the best parameters should involve an interactive fit. Such a procedure is not yet available for 2D spectra, and instead, we carried out a wide range of numerical simulations to explore the precision of the “best fit” parameters in Figure 3b. We found that changes in  $\tau_g$  by  $\pm 20$  fs from the optimal value of 70 fs gave very different evolution of the antidiagonal width. Likewise, a change of  $\lambda$  or  $\sigma$  by 10% from their optimal values led to clearly visible changes in the evolution of the diagonal width or the slope of the nodal line.

Significant, almost uniform ADW broadening during first 50 fs arises from both “improperly ordered” sequences of light matter interaction during laser pulse overlap<sup>25</sup> and exciton relaxation and exciton energy fluctuations. Figure 3c shows the ADW of the absolute 2D spectra simulated with the same parameters as in Figure 3b, except that exciton relaxation was not included during population time  $T$ . In this case, the ADW increases nonuniformly during the first 50 fs with greater broadening at low frequencies and then becomes constant at longer population times,  $T$ . Thus, the uniform greater increase of the ADW in Figure 3b indicates that relaxation processes contribute to nonuniform ADW broadening (with higher frequencies broadening more) during first 50 fs. The ADW evolution (Figure 3b) for population times longer than 50 fs is thus mostly defined by the exciton relaxation.

As we will see in the discussion of Figure 4, relaxation rates are faster for higher-lying states within the absorption band.

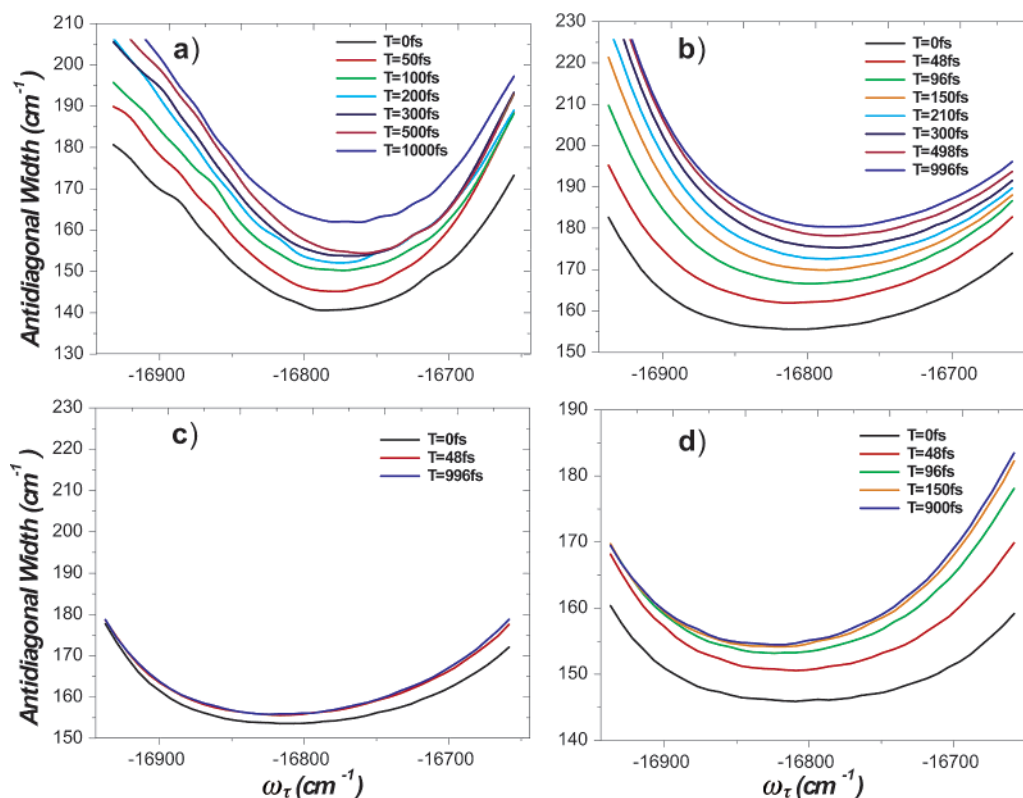


**Figure 3.** Effects of the exciton relaxation and spectral diffusion on the evolution of the absolute 2D spectrum. Antidiagonal width of the absolute 2D spectrum as a function of frequency  $\omega_\tau$  plotted for population times indicated on plots: (a) experiment, (b) simulation including exciton population relaxation (simulation parameters are the same as in Figures 1 and 2), (c) simulation same as in (b) but without exciton population relaxation during population time  $T$ , and (d) simulation without exciton relaxation but slow ( $\tau_g = 130$  fs) solvation correlation function (see text for details).

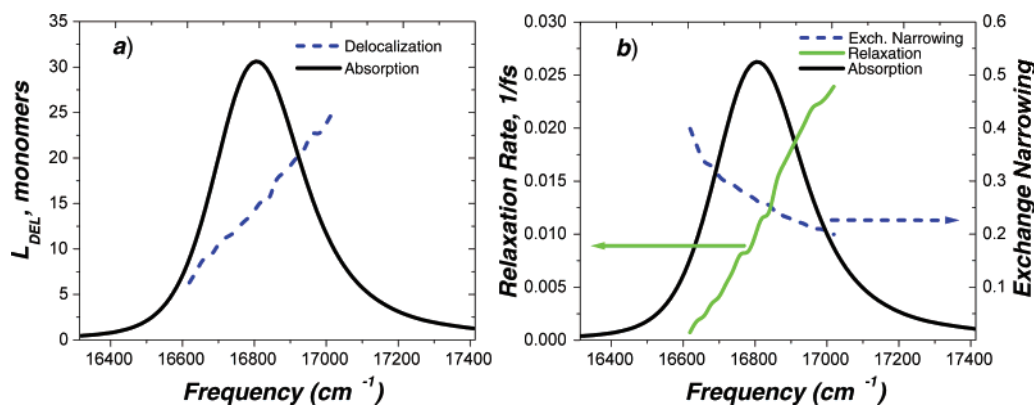


**Figure 4.** Variations of the exciton relaxation rates and delocalization lengths across the absorption spectrum of J-aggregates. (a) Exciton delocalization length (dashed line) plotted across simulated linear absorption spectrum (solid line) of the J-aggregates. (b) Exchange narrowing factor of the energy fluctuation of the exciton states (dashed) and one-exciton population relaxation rates from a given exciton state to all other exciton states (green line) plotted across simulated linear absorption spectrum (solid black line) of the J-aggregates. Simulation parameters in (a) and (b) are the same as in Figures 1, 2a, and 3b.

This induces stronger population transfer induced broadening at the higher-frequency region of the ADW plots in Figure 3a and b when  $T$  increases from 50 to 500 fs. At longer population times, the ADW increases more at lower frequencies resulting from relaxation among lower-lying states. At this point, the population of higher-lying states has reached thermal equilibrium, and no further evolution is observed for the higher frequencies.

In the absence of the energy transfer during  $T$ , nuclear-motion-induced energy gap fluctuation dynamics leads to distinctively different ADW evolution (Figure 3d). In these simulations, we used the same parameters as in Figure 3b, however, with a slower monomer correlation function ( $\lambda = 200$   $\text{cm}^{-1}$ ,  $\tau_g = 130$  fs) and no energy transfer during  $T$ . In this

case, the ADW increases significantly over the first 50 fs (with slightly stronger broadening at low frequencies). As the population time increases, the low-frequency part of the ADW increases more strongly than higher frequencies. The ADW stops increasing for population times significantly larger than  $T \sim \tau_g = 130$  fs. The reduced broadening of higher exciton states is caused by stronger exchange narrowing of the higher-lying (and more delocalized) exciton states (see discussion of Figure 4).

Thus, exciton energy fluctuation dynamics (described by diagonal exciton–phonon coupling Hamiltonian  $H_{kk}^{\text{ex-ph}}(q)$ ) have a larger impact on the lower-lying states and influence the low-energy part of ADW, while exciton relaxation (described by off-diagonal exciton–phonon coupling Hamiltonian

$H_{kk'}^{\text{ex-ph}}(q)$  significantly broadens the high-frequency region of the ADW at shorter population times  $T$  and the low-frequency region at longer population times.

Figure 4 shows the variation of the averaged exciton delocalization length  $L_{\text{DEL}}(k)$  of exciton  $k$  and exciton relaxation rates across the J-aggregate absorption spectrum for the simulations shown in Figures 1, 2, and 3b.  $L_{\text{DEL}}(k) = 1/\sum_{n=1}^N |\phi_{k,n}|^4$ , where the  $\phi_{k,n}$  are the coefficients of monomer states  $n$  in exciton state  $k$ . The averaging was performed by dividing the exciton energy axis into 20  $\text{cm}^{-1}$  wide bins and by averaging the values of the delocalization length and the relaxation rate within each bin.

The exciton delocalization length  $L_{\text{DEL}}(k)$  (Figure 4a) varies from  $\sim 6$  monomers at the low-frequency side of the absorption spectrum to  $\sim 25$  monomers at the high-frequency side. Delocalization induces averaging of the nuclear-motion-induced energy gap fluctuations of state  $|k\rangle$  by  $1/\sqrt{L_{\text{DEL}}(k)}$  (Figure 4b). Higher-energy exciton states are more strongly exchange-narrowed. Conversely, relaxation rates are faster on the higher-energy side of the absorption spectrum (Figure 4b).

In our model, the extent of the exciton delocalization,  $L_{\text{DEL}}(k)$ , is determined by the ratio  $\sigma/J$ .<sup>26</sup> Nuclear-motion-induced exciton energy fluctuations of delocalized exciton states (defined by the diagonal exciton–phonon coupling Hamiltonian  $H_{kk}^{\text{ex-ph}}(q)$ ) are reduced (or exchange-narrowed) by a factor of  $\sim 1/\sqrt{L_{\text{DEL}}(k)}$  with respect to those fluctuations in monomers. In a system with stronger disorder  $\sigma$ , the exciton energy fluctuations of more localized exciton states are stronger due to reduced exchange-narrowing, while exciton relaxation rates are reduced as the spatial overlap of exciton states with close energies is reduced in disordered systems.<sup>18</sup> Thus, a parameter  $\sigma/J$  is also responsible for partitioning of the electron–phonon Hamiltonian to diagonal  $H_{kk}^{\text{ex-ph}}(q)$  and off-diagonal  $H_{kk'}^{\text{ex-ph}}(q)$  parts.

In a system with larger disorder value  $\sigma$ , the number of exciton states with significant transition dipole moments to the ground state is larger, leading to broadening of the J-aggregate absorption spectrum. Both diagonal and off-diagonal parts of the exciton–phonon coupling Hamiltonian increase linearly with  $\lambda$ , thus a parameter  $\lambda/\sigma$  is responsible for the balance of static and dynamic broadening mechanisms to the J-aggregate spectra.

The time scale of the monomer solvation correlation function ( $\tau_g$ ) directly determines the time scale of the exciton energy fluctuation dynamics. The time scale of the exciton energy relaxation processes strongly depend on all model parameters and, in our case, occur on time scales faster and slower than  $\tau_g$ . The value of  $\tau_g$  affects the nature of the exciton-relaxation-induced population redistribution across the exciton absorption band. Relaxation between two exciton states occurs effectively if the energy gap between those states is smaller than the spectral width of the correlation function (which is related to  $1/\tau_g$ ). Thus, in a system with slower fluctuations, the population redistribution resulting from exciton relaxation occurs by smaller energy jumps.

## Conclusion

In summary, we show that the ultrafast heterogeneous dynamics in the exciton manifold can be recovered with 2D optical spectroscopy. We obtained a good agreement between the complete experimental third-order nonlinear response and the theoretical simulations based on self-consistent Frenkel exciton theory, including energetic monomer disorder, interchromophore electrostatic coupling, nuclear-motion-induced

electron–phonon coupling Hamiltonian, and implementing modified Redfield theory for calculations of population transfer within the exciton band. We show that exciton relaxation between the exciton states and nuclear-motion-induced exchange-narrowed energy fluctuations of individual delocalized exciton states lead to distinctively different evolution of the absolute 2D spectrum and hence their relative influences distinguished. Our technique also allows recovery of variations of exciton relaxation rates as well as exciton delocalization across the absorption band.

Knowledge of the frequency-dependent ultrafast exciton dynamics provides information on the nature of phonon coupling and on the structure of the exciton manifolds, allowing development and verification of electron–phonon coupling theories for nanostructures, peptides, and biological light-harvesting complexes.

**Acknowledgment.** This work is part of the thesis of I. Stiopkin, *Resonant Heterodyne Two-Dimensional Electronic Spectroscopy*, Columbia University, 2005. This work was supported by a grant from the National Science Foundation. T.B. thanks the German Science Foundation (DFG) for an Emmy Noether Fellowship. We thank Samar Metha and Prof. Vladimir Chernyak for many helpful discussions.

## References and Notes

- (1) Manzoni, C.; Gambetta, A.; Menna, E.; Meneghetti, M.; Lanzani, G.; Cerullo, G. *Phys. Rev. Lett.* **2005**, *94*.
- (2) Shabaev, A.; Efros, A. L. *Nano Lett.* **2004**, *4*, 1821.
- (3) Ellington, R. J.; Beard, M. C.; Johnson, J. C.; Yu, P. R.; Micic, O. I.; Nozik, A. J.; Shabaev, A.; Efros, A. L. *Nano Lett.* **2005**, *5*, 865.
- (4) Brixner, T.; Stenger, J.; Vaswani, H. M.; Cho, M.; Blankenship, R. E.; Fleming, G. R. *Nature (London)* **2005**, *434*, 625.
- (5) Bednarz, M.; Malyshev, V. A.; Knoester, J. *Phys. Rev. Lett.* **2003**, *91*.
- (6) Rubtsov, I. V.; Wang, J. P.; Hochstrasser, R. M. *Proc. Natl. Acad. Sci. U.S.A.* **2003**, *100*, 5601.
- (7) Moll, J.; Daehne, S.; Durrant, J. R.; Wiersma, D. A. *J. Chem. Phys.* **1995**, *102*, 6362.
- (8) Ohta, K.; Yang, M.; Fleming, G. R. *J. Chem. Phys.* **2001**, *115*, 7609.
- (9) Jonas, D. M. *Annu. Rev. Phys. Chem.* **2003**, *54*, 425.
- (10) Golonzka, O.; Khalil, M.; Demirdoven, N.; Tokmakoff, A. *Phys. Rev. Lett.* **2001**, *86*, 2154.
- (11) Woutersen, S.; Hamm, P. *J. Phys. Chem. B* **2000**, *104*, 11316.
- (12) Asplund, M. C.; Zanni, M. T.; Hochstrasser, R. M. *Proc. Natl. Acad. Sci. U.S.A.* **2000**, *97*, 8219.
- (13) Mukamel, S. *Annu. Rev. Phys. Chem.* **2000**, *51*, 691.
- (14) Tian, P. F.; Keusters, D.; Suzuki, Y.; Warren, W. S. *Science* **2003**, *300*, 1553.
- (15) Cowan, M. L.; Bruner, B. D.; Huse, N.; Dwyer, J. R.; Chugh, B.; Nibbering, E. T. J.; Elsaesser, T.; Miller, R. J. D. *Nature (London)* **2005**, *434*, 199.
- (16) Asbury, J. B.; Steinel, T.; Stromberg, C.; Gaffney, K. J.; Piletic, I. R.; Goun, A.; Fayer, M. D. *Phys. Rev. Lett.* **2003**, *91*.
- (17) Blankenship, R. E. *Molecular Mechanisms of Photosynthesis*; Blackwell Science: Cambridge, MA, 2001.
- (18) Zhang, W. M.; Meier, T.; Chernyak, V.; Mukamel, S. *J. Chem. Phys.* **1998**, *108*, 7763.
- (19) Yang, M. N.; Fleming, G. R. *Chem. Phys.* **2002**, *275*, 355.
- (20) Brixner, T.; Stiopkin, I. V.; Fleming, G. R. *Opt. Lett.* **2004**, *29*, 884.
- (21) Brixner, T.; Mancal, T.; Stiopkin, I. V.; Fleming, G. R. *J. Chem. Phys.* **2004**, *121*, 4221.
- (22) Johnson, A. E.; Kumazaki, S.; Yoshihara, K. *Chem. Phys. Lett.* **1993**, *211*, 511.
- (23) Fidder, H.; Knoester, J.; Wiersma, D. A. *J. Chem. Phys.* **1991**, *95*, 7880.
- (24) Lang, M. J.; Jordanides, X. J.; Song, X.; Fleming, G. R. *J. Chem. Phys.* **1999**, *110*, 5884.
- (25) Joo, T. H.; Jia, Y. W.; Yu, J. Y.; Lang, M. J.; Fleming, G. R. *J. Chem. Phys.* **1996**, *104*, 6089.
- (26) Knoester, J. *Phys. Rev. A* **1993**, *47*, 2083.